RSC Advances

ROYAL SOCIETY OF CHEMISTRY

www.rsc.org/advances

Three dimention MnO_2/graphene/carbon nanotubes-based non-noble-metal bifunctional electrocatalyst for oxygen reduction and water oxidation

Daixin Ye[a], Tong Wu[a], Hongmei Cao[a], Yong Li[b], Yi Wang[a], Baohong Liu[a], Song Zhang[a], Jilie Kong[a*]

[a]*Department of Chemistry and Institutes of Biomedical Sciences, Fudan University, Shanghai 200433, PR China*

[b]*Shanghai Institute of Space Power-sources, Shanghai, PR China*

Abstract: The electrochemical oxygen reduction reaction (ORR) and oxygen evolution reaction (OER) are of great interest as their processes involved in energy conversion between fuel and electricity. Here, we developed a bifunctional noble metal-free electrocatalyst MnO_2/graphene/carbon nanotubes which could be a promising candidate for such electrocatalysts. It can act as efficient cathode catalyst for the ORR with a positive half-wave potential only ~55 mV deviation from commercial Pt/C and high cathodic current density which is comparable to the Pt/C catalyst. Moreover, the hybrid exhibits superior durability with nearly no decay in ORR activity even over 10,000 s of continuous operation in 0.1 M KOH, while Pt/C shows 20% decrease in the activity. The most importantly, the hybrid is also highly active for OER, making it a high-performance non-precious metal-based bi-catalyst for both ORR and OER.

Keywords: oxygen evolution reaction; oxygen reduction reaction ; MnO_2; Graphene;

* Corresponding author. Address: Department of Chemistry and Institutes of Biomedical Sciences, Fudan University, Shanghai 200433, PR China. Tel.: +86 21 65642138 ; fax: +86 21 65641740
E-mail address: jlkong@fudan.edu.cn

Carbon nanotube

1. Introduction

Oxygen electrochemistry has attractted growing interest as conversions between O_2 and H_2O as it plays important roles in renewable energy technologies. The oxygen reduction reaction (ORR) is the ubiquitous cathode reaction in fuel cells, while the oxygen evolution reaction (OER) is the anode reaction employed in electrolysis cell[1]. Both the fuel cell reaction and the water electrolysis reaction require large over-potentials at the oxygen electrode – no current catalyst material operates a near the equilibrium potential for either the ORR or the OER. [2] ORR takes place almost exclusively on Pt/C catalysts at the cathode in lithium–air batteries and low-temperature fuel cells. However, the high price, sluggish ORR process, intolerance to fuel crossover, and instability of the Pt/C catalyst in the fuel-cell environment have greatly impeded the commercialization and limited their performance[3, 4]. At the same time, Pt has only moderate activity for the OER. Ruthenium (Ru) and iridium (Ir) oxides are the OER catalysts with moderate over-potentials, but they still have some shortages. Thus, bifunctional catalyst development satisfying significant overpotentials for both reactions and exclusive precious metals that are both scarce and expensive would be a major challenge. Therefore, to develop efficient bifunctional catalysts for both ORR and OER are highly urgent, particularly for unitized regenerative fuel cells, a promising energy storage system that works as a fuel cell and in reverse as a water electrolyzer producing H_2 and O_2 to feed the fuel cell.

In this respect, we apply a facile one-pot reaction process to synthesis of MnO_2/graphene/carbon nanotubes as efficient bifunctional oxygen catalysis. Manganese oxides have been widely investigated for their prominent advantages arise from low cost and toxicity as well as high chemical stability and catalytic activity[5-9]. More importantly, manganese oxide surfaces and molecular mimics are potentially interesting materials for bifunctional oxygen catalysis[1]. However, the poor conductivity of MnO_2 ($\sim 1 \times 10^5$ S/cm) limits its applications. In order to enhance the electrical conductivity of MnO_2 electrodes, tremendous efforts have been focused on combining highly conductive materials such as graphene, carbon nano-tubes, porous carbon, and activated carbons[10-12]. Herein, a hybrid carbon matrix: CNT matrix and partly exfoliated graphene came from the walls of CNT matrix not only provides large surface area but also highly improves the conductivity due to the bridging role of CNT among graphene. Meanwhile, the metal nanoparticles strongly coupled with the supports to exert the synergistic effects and also to escape from the detachment, aggregation and even dissolution during potential cycling which was extremely beneficial for the stability. Therefore, the fabricated MnO_2/graphene/carbon nanotubes exhibits surprisingly high performance in both ORR and OER even comparable catalytic activity to a commercial carbon-supported Pt catalyst in alkaline solutions. Simultaneously, the hybrid also shows superior stability, thus giving rise to a new bi-functional catalyst for ORR and OER.

2. Experimental

2.1 Apparatus and reagents

All experiments were performed in 0.1 M KOH and doubly distilled water was used throughout.

Electrochemical experiments including cyclic voltammetry (CV), linear sweep voltammetry (LSV) and amperometry were carried out on CHI 660C electrochemical workstation (Chenhua, Shanghai, China). A conventional three-electrode electrochemical system was used for all electrochemical experiments, which consisted a working electrode, a Pt foil auxiliary electrode and a saturated calomel electrode. A glassy carbon electrode (GCE) was used as the basal working electrode. Transmission electron microscopy (TEM) images were taken with a JEOL2011microscope (Japan) operated at 200 kV. Raman spectra were recorded on a LabRam-1B microscopic confocal Raman spectrometer (Jobin Yvon, France). Powder X-ray diffraction (XRD) measurements were performed on a Bruker D4 diffractometer at a scanning rate of min 1°/min in the 2θ range from 10 to 80° (Cu Kα radiation, λ= 1.54056 Å). Thermogravimetric analysis (TG) of the sample was performed on a Pyris Diamond TG/DTA thermo-gravimetric analyzer (Perkin-Elmer Thermal Analysis).

2.2 Preparation of MnO_2/G/CNT hybrid

MnO_2/G/CNT hybrid was prepared by one pot method. In a typical procedure, MWCNTs (10 mg) were dispersed in 10 mL water including 100 μL H_2SO_4 and 400 μL HNO_3 under stirring at 70℃ for 30 min. Afterwards, 300 μL H_2SO_4 was added into the above mixture and keeped in 0℃ for 1 h. At last, permanganate crystallites (50 mg) were added and stirred at 55℃ for 2 h. The reaction mixture was then

removed from the heat source, and poured into 500 mL of doubly distilled water to cool down and dilute. The solution was filtered over a polytetrafluoroethylene membrane (0.22 μm pore size, Aldrich), and the remaining solid was washed repeatedly with distilled water for several times. The obtained products were called MnO_2/G/CNT/GCE.

C/MnO_2 was synthetized using graphite and permanganate, and the specific process was the same as the procedure for synthesis of MnO_2/G/CNT.

2.3 Preparation of modified electrodes and electrochemical test

Prior to use, the glassy carbon rotating disc electrode (GCRDE) was polished with 0.3 and 0.05 μm α-Al_2O_3 powder until a mirror-shiny surface was obtained, then ultrasonicated in ethanol and doubly distilled water for 10 min, respectively. Finally, it was dried in the stream of high purity nitrogen for further use. 2 mg of the MnO_2/G/CNT samples were dispersed in a solution containing 1 mL of deionized water and 0.5 mL of 1 wt.% Nafion aqueous solution. The mixture was ultrasonicated to obtain a homogenous catalyst ink. Then 10 μL of the resulting mixture was dropped onto the cleaned GCRDE surface to prepare MnO_2/G/CNT/GCE, C/MnO_2/GCRDE, or CNT/GCRDE and the modified electrode was allowed to dry under an infrared lamp for 10 min. The obtained modified electrodes were preserved in a refrigerator at 4℃ after being washed with doubly distilled water.

Before test, an O_2/N_2 flow was used through the electrolyte in the cell for 20 min to saturate it with O_2/N_2. The cell was kept in a 25 ºC water bath for all the electrochemical tests. The linear sweep voltammograms of the modified GCRDE

were recorded in O_2 saturated 0.1 M KOH with a scan rate of 5 mV s^{-1} at various rotating speeds from 225 to 1600 rpm.

3 Results and discussion

3.1 Characterization of MnO_2/G/CNT hybrid

Fig. 1A, Fig. 1SA and Fig. 1SB present the TEM images of the MnO_2/G/CNT, which display a long-range array of transparent petal-like sheets. **High resolution TEM image (Fig. 1SA) showed that the MnO_2 nanorod (with a diameter of 4.6-5.9 nm, and length of 45-54 nm) mainly located at the surface of the graphene and closely attached on the stripped graphene.** Fig. 1B shows SEM images of the hybrid, with the morphology of reticular and curved petal-like walls on the carbon nanotubes over the entire longitudinal length. To get further insight into the structure of the hybrid, excess of permanganate and MnO_2 was removed. Sufficient amount of hydrogen peroxide and 1 M HCl solution were added the samples and then washed by large amount of distilled water repeatedly. Fig. S2A shows TEM image of the samples after the remove of MnO_2, revealing that the tidy petals structure collapsed without the support of MnO_2 but the stripped graphene still can be seen around the CNT. We used Raman technique to investigate the vibrational properties of the treated samples (Fig. S2B). Comparing to the samples without treatment, the Raman result shows the obvious characteristic peaks located at 640 cm^{-1} disappeared, demonstrating that the large amount of MnO_2 nanocrystals were destroyed after treatment. Raman spectra of the MnO_2/G/CNT and CNT are displayed in Fig. 1C. Both CNT and MnO_2/G/CNT

display two prominent peaks at 1573 and 1325 cm^{-1}, which correspond to the well-documented G and D bands, respectively. Intensity ratio of D to G band (I_d/I_g) increases accordingly from 0.13 to 0.38 with the oxidation reaction progress, indicating the enhanced level of disorder of the product and the formation of sp3 carbon after functionalization. Raman band at 640 cm^{-1} can be recognized as the symmetric stretching vibration (Mn–O) of the MnO_6 groups[13], which can be used to characterize the tunnel species of α-type MnO_2 materials. The XRD patterns of the MnO_2/G/CNT and prinst CNT are shown in Fig. 1D. Compared with the standard XRD pattern of MnO_2 (JCPDS 44-0141), the observed reflections of 28.82°, 37.44°, 41.94°, 49.83°, 56.39°, 60.27°, 69.69° were identified. The experimentally obtained peaks of 26.33° is ascribed to the crystal plane of graphite, which is consistent with the XRD pattern of CNT (Fig. 1C). The results indicate that the final product is composed of crystal MnO_2 and CNT. Typical XPS spectra for the MnO_2/G/CNT are shown in Fig. 1E and F. The peaks of Mn (2p3/2,2p1/2), O 1s and C 1s can be observed in the survey spectrum. Furthermore, the Mn $2p_{3/2}$ peak is centered at 643.2 eV and the Mn $2p_{1/2}$ peak is located at 654.6 eV, with a spin-orbit splitting of 11.4 eV, suggesting that the predominant manganese oxidation state is Mn(IV). These results are in accordance with the previous reports[14].

Fig. 2A shows a TEM image of a representative segment of the hybrid. Fig. 3B–D shows elemental distribution of Mn, O and C in the hybrid. The mapping results indicate that the distribution of C, Mn and O elements is homogeneous throughout the petal-like nanosheets, implying that the nanosheets are composed of manganese oxide

and C. To further get the relative content of MnO_2 in the hybrid, thermogravimetric (TG) was done in air and the curve was show in Fig. 3. The content of the of MnO_2 in the hybrids was 52.9 wt% according to the TG curve.

3.2 Electrocatalytic properties toward the ORR

First of all, to gain insight into the ORR activity of MnO_2/G/CNT/GCRDE, we examined the electrocatalytic properties of MnO_2/G/CNT/GCRDE in a N_2- and O_2-saturated 0.1 M aqueous KOH electrolyte solution using cyclic voltammetry at a scan rate of 100 mV s^{-1} (Fig. 4A). A quasi-rectangular voltammogram without obvious redox peak was obtained when the electrolyte was saturated with N_2. In contrast, when the electrolyte was saturated with O_2, the MnO_2/G/CNT hybrid showed a well-defined characteristic ORR peak with a cathodic peak at 0.7 V (*vs*. RHE), suggesting a pronounced electrocatalytic activity of the MnO_2/G/CNT hybrid modified GCRDE for oxygen reduction. For the purpose of comparison, the LSV curves for the commercial catalyst (Pt/C, 20 wt%), MnO_2/G/CNT, C/MnO_2, CNT are shown in Fig. 4B. The same amount of each catalyst by mass (0.068 mg cm^{-2}) was loaded onto each GCRDE. It is seen that the onset potential of the MnO_2/G/CNT hybrid electrode towards ORR is close to that of Pt/C, whereas C/MnO_2, CNT electrodes commence its oxygen reduction at more negative potentials. Moreover, the plateau limiting currents of MnO_2/G/CNT **(3.76 mA cm^{-2})** are much larger than those of CNT, C/MnO_2 and even comparable to that of Pt/C, which is possibly attributed that MnO_2/G/CNT has larger electroactive surface area and the synergistic effect generated from MnO_2, G, CNT. Meanwhile, **manganese oxide itself is known to**

have considerable activity for the ORR/OER reactions.[15, 16] Also, the structure of G/CNT favours the electron transfer and then boost ORR activity.

3.3 Kinetics, stability and anti-poisoning properties study

To obtain additional insight about the ORR process on MnO_2/G/CNT hybrid, LSVs on GCRDE were recorded at different rotating speeds from 0 rpm to 2000 rpm in 0.1 M KOH electrolyte saturated with O_2 (Fig. 5A); In Fig. 5B, good linear fitting can be seen for each potential with the identical slopes. For the oxygen reduction on an GCRDE, Koutecky-Levich (K–L) plots were analyzed at different electrode potentials. The kinetic parameters can be analyzed on the basis of the K–L equations.

$$J^{-1}=J_L^{-1}+J_K^{-1} \quad (1)$$

$$J_L = 0.62nFC_0D^{2/3}v^{-1/6}w^{1/2} \quad (2)$$

$$J_K = nFkC_0 \quad (3)$$

where J is the current density, J_K and J_L are the kinetic- and diffusion-limiting current densities, w is the angular velocity of the disk ($w = 2\pi N$, N being the rotation frequency), n is the overall number of electrons transferred upon oxygen reduction, F is the Faraday constant (F = 96 485 C mol^{-1}), D is the diffusion coefficient of O_2 in 0.1 M KOH electrolyte (1.9×10^{-5} cm^2 s^{-1}), C_0 is the bulk concentration of O_2 (1.2×10^{-3} mol L^{-1}), v is thekinetic viscosity of the electrolyte (0.01 cm^2 s^{-1}) and k is the electron transfer rate constant.

The slopes of their best linear fit lines were used to calculate the number of electrons transferred (n), which was calculated to be 3.95, 4.00, 3.98, and 3.96 at 0.8, 0.75, 0.7, 0.65 and 0.6 V, respectively, suggesting MnO_2/G/CNT hybrid favours a 4e

oxygen reduction process, similar to ORR catalysed by a high-quality commercial Pt/C catalyst measured in the same 0.1 M KOH electrolyte (n~4 for Pt/C) (Fig. 5C, D). **So, according to the reported work[16], we infer that the possible mechanism for ORR maybe as follows:**

$MnO_2 + H_2O + e^- \leftrightarrow MnOOH + OH^-$ (1)

$2MnOOH + O_2 \leftrightarrow (MnOOH)_2{-}{-}{-}O_{2,ads}$ (2)

$(MnOOH)_2{-}{-}{-}O_{2,ads} + e^- \rightarrow MnOOH{-}{-}{-}O_{ads} + OH^- + MnO_2$ (3)

$MnOOH{-}{-}{-}O_{ads} + e^- \leftrightarrow MnO_2 + OH^-$ (4)

$(MnOOH)_2{-}{-}{-}O_{2,ads}$ represents each oxygen molecule adsorbs onto two neighboring MnOOH sites. In such a process, the Mn^{III}/Mn^{IV} species act as oxygen acceptor/donor.

The RDE measurements for the C/MnO_2 and MWCNT electrocatalyst were also carried out in our experiments. As seen from Supporting Information Fig. S3, C/MnO_2 has a electron transfer number of ~4. MWCNT also has an ORR response, but its activity is less than desirable. The numbers of electrons transferred per O_2 for MWCNT is calculated to be 2.38, 1.7, and 1.8 at 0.6, 0.5 and 0.4 V, respectively (Fig. S4). This suggests that the oxygen reduction on MWCNT electrocatalyst may proceed by a coexisting pathway involving both the two-electron and four-electron transfers.

Fig. 6 shows the stability of MnO_2/G/CNT and Pt/C for ORR. It can be seen that the current for ORR at the Pt/C electrode exhibited nearly 20% decrease in activity over **40,000 s** of continuous operation in 0.1 M KOH (Fig. 6), while our hybrid exhibits superior durability to Pt/C catalyst in 0.1 KOH, with little decay in ORR

activity, giving higher long-term ORR currents than the stable currents sustained by the Pt/C electrode.

To examine possible crossover effects, the electrocatalytic selectivity of MnO_2/G/CNT hybrid was measured against the electro-oxidation of methanol in 0.1 M KOH saturated with O_2 shown in Fig. 7. No noticeable change was observed in the oxygen-reduction current compared to MnO_2/G/CNT in O_2 saturated 0.1 M KOH without methanol. Thus, MnO_2/G/CNT hybrid exhibited high selectivity to avoid crossover effects for the ORR.

3.4 Electrocatalytic properties toward the OER

At last, we extended the potential of our hybrid electrode to 2.25 V versus RHE to the water oxidation regime and evaluated electrocatalytic oxygen evolution reaction (OER). Regarding OER activity, MnO_2/G/CNT hybrid was clearly more active than Pt/C and C/MnO_2. From Fig. 8, MnO_2/G/CNT was found to be highly active for both the ORR and the OER. These results make our hybrid material a powerful bi-functional catalyst for both oxygen reduction and water oxidation.

4. Conclusion

To sum up, we fabricated an inexpensive and earth-abundant catalyst -MnO_2/G/CNT hybrid, which exhibited excellent bifunctional oxygen electrode activity. The special features of MnO_2/G/CNT hybrid and large active surface areas that accelerate the interfacial electrochemical reaction, contributing to their potent

ORR and OER activities. Furthermore, such a catalyst could comparable to fresh commercial Pt/C catalyst in ORR and OER activities in alkaline solution but far exceeding Pt/C in stability. Based on this, OER activities can be further improved by synergistic coupling of nonprecious functional materials, which is highly required for energy conversion technologies.

5. Acknowledgments

This work was supported by The National Natural Science Foundation of China (21175029, 21335002) and the Shanghai Leading Academic Discipline Project (B109).

References:

1. Y. Gorlin and T. F. Jaramillo, *J Am Chem Soc*, 2010, **132**, 13612-13614.
2. G. Y. Chen, S. R. Bare and T. E. Mallouk, *J Electrochem Soc*, 2002, **149**, A1092-A1099.
3. R. Bashyam and P. Zelenay, *Nature*, 2006, **443**, 63-66.
4. M. Lefevre, E. Proietti, F. Jaouen and J. P. Dodelet, *Science*, 2009, **324**, 71-74.
5. G. H. Yu, L. B. Hu, M. Vosgueritchian, H. L. Wang, X. Xie, J. R. McDonough, X. Cui, Y. Cui and Z. N. Bao, *Nano Lett*, 2011, **11**, 2905-2911.
6. F. Y. Cheng, J. Shen, W. Q. Ji, Z. L. Tao and J. Chen, *ACS Appl Mater Inter*, 2009, **1**, 460-466.
7. L. Trahey, N. K. Karan, M. Chan, J. Lu, Y. Ren, J. Greeley, M. Balasubramanian, A. K. Burrell, L. A. Curtiss and M. M. Thackeray, *Adv Energy Mater*, 2013, **3**, 75-84.
8. G. Y. Zhu, Z. He, J. Chen, J. Zhao, X. M. Feng, Y. W. Ma, Q. L. Fan, L. H. Wang and W. Huang, *Nanoscale*, 2014, **6**, 1079-1085.
9. Y. Hou, Y. W. Cheng, T. Hobson and J. Liu, *Nano Lett*, 2010, **10**, 2727-2733.
10. G. H. Yu, L. B. Hu, N. A. Liu, H. L. Wang, M. Vosgueritchian, Y. Yang, Y. Cui and Z. A. Bao, *Nano Lett*, 2011, **11**, 4438-4442.
11. Z. J. Fan, J. Yan, T. Wei, L. J. Zhi, G. Q. Ning, T. Y. Li and F. Wei, *Adv Funct Mater*, 2011, **21**, 2366-2375.
12. Y. Chen, Y. Zhang, D. Geng, R. Li, H. Hong, J. Chen and X. Sun, *Carbon*, 2011, **49**, 4434-4442.
13. S. Ma, K. Ahn, E. Lee, K. Oh and K. Kim, *Carbon*, 2007, **45**, 375-382.
14. Z. Liu, X. Tan, X. Gao and L. Song, *J Power Sources*, 2014, **267**, 812-820.
15. J. Feng, Y. Liang, H. Wang, Y. Li, B. Zhang, J. Zhou, J. Wang, T. Regier and H. Dai, *NANO RESEARCH*, 2012, **5**, 718-725.
16. I. Roche, E. Chainet, M. Chatenet and J. Vondrak, *JOURNAL OF PHYSICAL CHEMISTRY C*, 2007, **111**, 1434-1443.

Figure captions:

Fig. 1 Characterization of MnO_2/G/CNT hybrid: (A) TEM image of the hybrid; (B) SEM image of the hybrid; (C) Raman spectra of the hybrid; (D) XRD patterns of the hybrid; (E) XPS survey spectra; (F) Mn 2p XPS spectra of MnO_2.

Fig. 2 (A) TEM image of a representative hybrid segment; (B-D) EDX mapping results for Mn, O and C elements.

Fig. 3 TG analysis of MnO_2/G/CNT.

Fig. 4 (A) CV of MnO_2/G/CNT hybrid mdified GCE in 0.1 M KOH with O_2 (red) and N_2 (black) saturation; (B) LSVs of different materials in O_2-saturated 0.1 M KOH with a sweep rate of 5 mV/s at a rotate rate of 1600 rpm.

Fig. 5 (A) LSVs of MnO_2/G/CNT at different rotating rates in 0.1 M KOH solutions saturated with O_2 (B) K-L plots of j^{-1} *vs* $\omega^{1/2}$ obtained from the LSV data at different potentials.

Fig. 6 Chronoamperometric responses of MnO_2/G/CNT and Pt/C modified electrodes kept at 0.74 V versus RHE in O_2-saturated 0.1 M KOH.

Fig. 7 CVs of MnO_2/G/CNT in O_2-saturated 0.1 M KOH and O_2-saturated 0.1 M KOH with 1 M methanol.

Fig. 8 Oxygen electrode activities within the ORR and OER potential window of C/ MnO_2 and MnO_2/G/CNT in O_2-saturated 0.1 M KOH.

Fig. 1

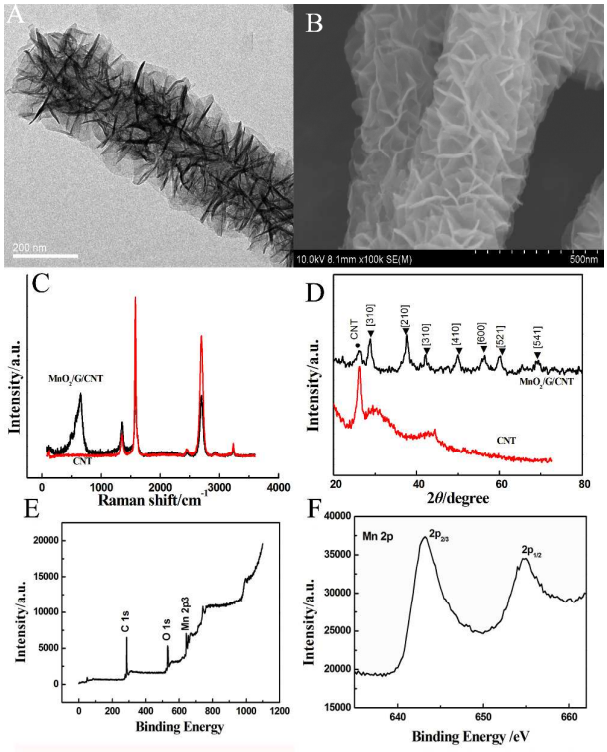

Fig. 2

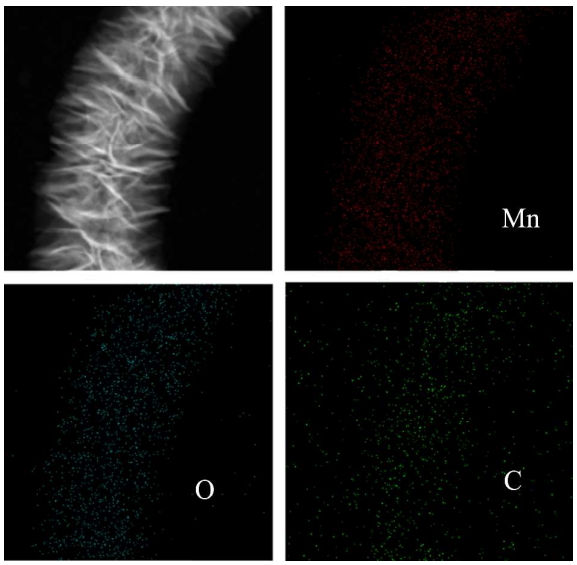

Fig. 3

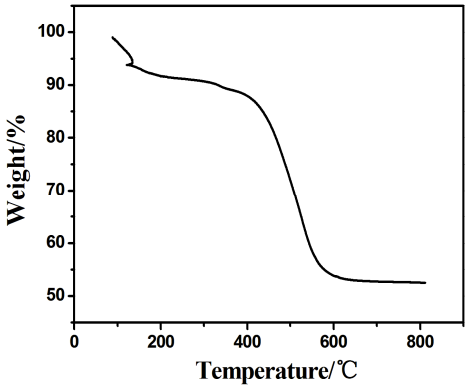

Fig. 4

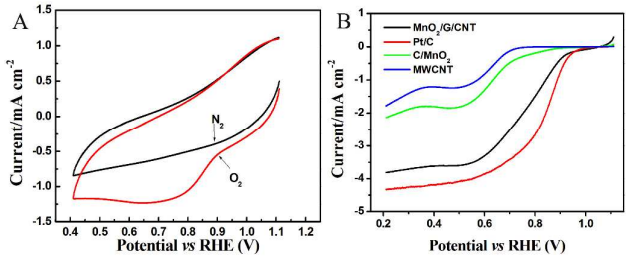

Fig. 5

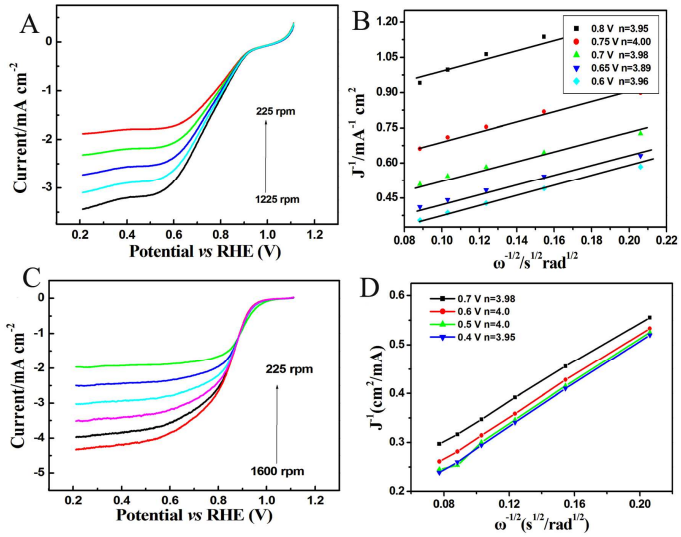

Fig. 6

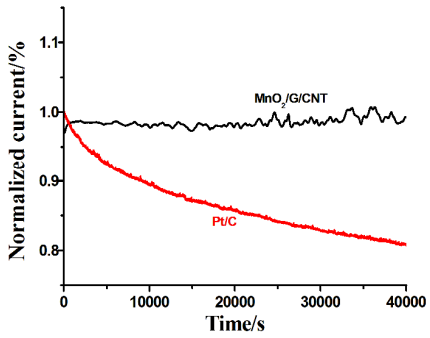

Fig. 7

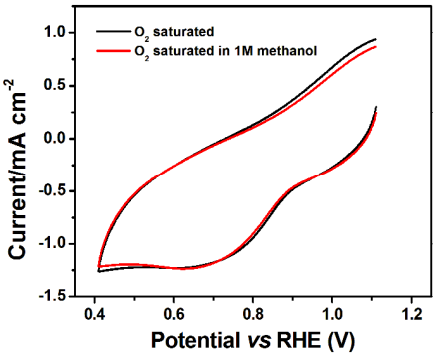

Fig. 8